

# Production of a Beam of isomeric $^{26}\text{Al}$ for Astrophysical Research

Olivier Grasdijk  
*Bachelor Thesis*  
KVI  
*Rijksuniversiteit Groningen*

July 27, 2011

ROSAT Dezember 2003

Max-Planck-Institut für  
extraterrestrische Physik

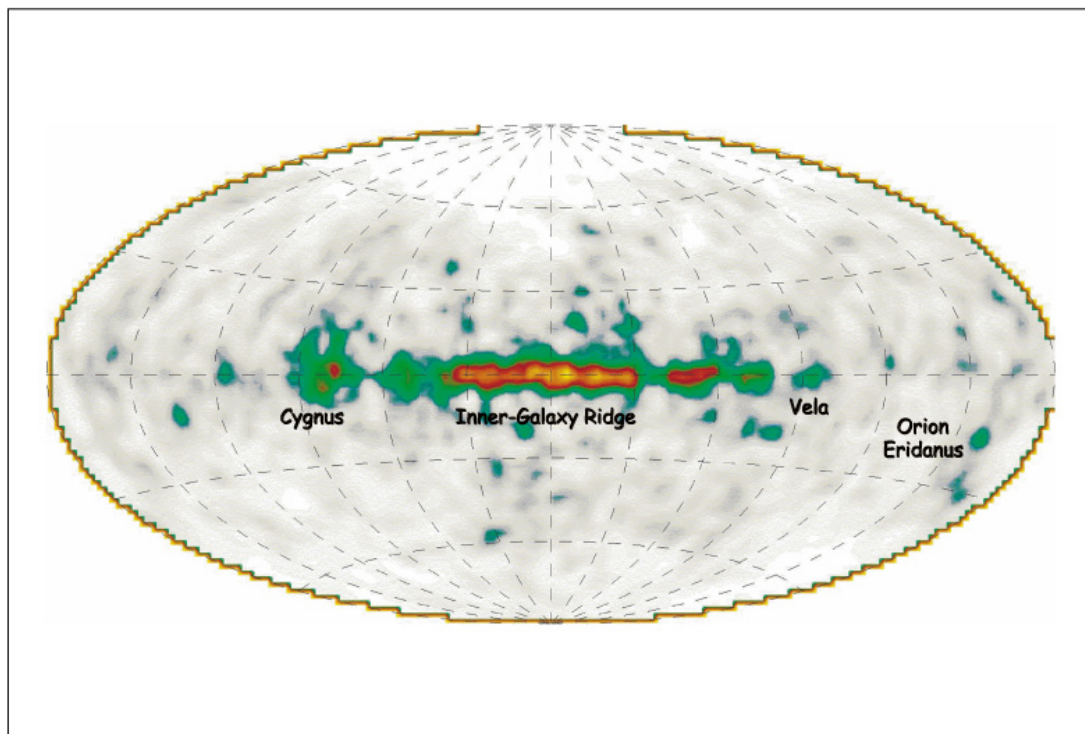


Figure 1: Sky map of the 1809 MeV  $\gamma$  line of  $^{26}\text{Al}$ [4]

## Abstract

In this work the production rate of the isomeric aluminum isotope  $^{26}\text{Al}^m$  was measured. This isomer lives only 6.3s. A beam of these isotopes needs to be produced to make nuclear reaction studies with this isomer possible. Only in this way a complete description of the nuclear synthesis process involving  $^{26}\text{Al}$  can be obtained. Using the AGOR cyclotron a primary  $^{26}\text{Mg}$  beam first hits a hydrogen target producing  $^{26}\text{Al}^m$  and other products. A magnetic separator is then used to separate the primary beam and most other products from the isomer. This study shows that for a typical beam of 100 nA  $^{26}\text{Mg}$ ,  $1.25 \times 10^6$ /second  $^{26}\text{Al}^m$  isotopes can be produced. The obtained secondary beam of  $^{26}\text{Al}^m$  has intensity sufficient to study astrophysical relevant nuclear reactions. However, a full separation of  $^{26}\text{Al}$  and contaminants could not be made.

# Contents

<b>1</b>	<b>Introduction</b>	<b>3</b>
<b>2</b>	<b>Expected Production of <math>^{26}\text{Al}</math></b>	<b>4</b>
<b>3</b>	<b>Detectors</b>	<b>6</b>
3.1	Annihilation Detectors . . . . .	6
3.1.1	Calibration . . . . .	6
3.2	Energy Detectors . . . . .	6
3.2.1	Calibration . . . . .	7
3.3	ToF Detection . . . . .	7
<b>4</b>	<b>Experiment</b>	<b>8</b>
<b>5</b>	<b>Data Analysis</b>	<b>8</b>
5.1	Intermediate Focal Plane . . . . .	8
5.2	Final Focal Plane . . . . .	9
5.3	Back to the Intermediate Focal Plane . . . . .	11
<b>6</b>	<b>Conclusion</b>	<b>13</b>
<b>7</b>	<b>Acknowledgements</b>	<b>13</b>

# 1 Introduction

The aluminum isotope  $^{26}\text{Al}$  is a source of  $\gamma$  emission in the galaxy.  $^{26}\text{Al}$  is used to study ongoing nucleosynthesis in the universe, because it has a short half-life ( $\tau_{1/2} = 0.717$  Myr [9]) compared to Galactical Chemical evolution ( $\sim\text{Gyr}$ ). It is produced in supernovae, AGB stars, Wolf Rayet stars[8] and ONe novae.

$^{26}\text{Al}$  decays (see fig. 2) via  $\beta^+$  emission to  $^{26}\text{Mg}$  in an excited state, and then drops to the ground state  $^{26}\text{Mg}^g$  under emission of a 1.809 MeV  $\gamma$ -ray.

Until 1954 it was thought that the half-life of  $^{26}\text{Al}$  was 6.3s and decays directly to the ground state [9]. However this was the isomeric  $^{26}\text{Al}^m$  state, not the ground state. By bombarding  $^{25}\text{Mg}$  and  $^{26}\text{Mg}$  with deuterons in the cyclotron of the University of Pittsburgh it was determined that the ground state has a half life of  $10^6$  s[12].

We want to look at  $^{26}\text{Al}^m$  to gain a better understanding of the processes that govern the destruction of  $^{26}\text{Al}$  in the galaxy. A request for beam time was made by a group of nuclear astrophysicists.[7]

In this experiment we are looking to see whether the production rate in the  $^{26}\text{Mg}(p,n)^{26}\text{Al}^m$  reaction is high enough to use the isomer as a radioactive beam to study reactions with  $^{26}\text{Al}^m$  as beam isotopes. The proposal is about measuring the  $^{26}\text{Al}^m(p,\gamma)^{27}\text{Si}$  cross sections, but reaction is very small, with a cross section in order  $\mu\text{b}$ . So instead they want to measure the  $^{26}\text{Al}^m(d,p)^{27}\text{Al}$  reaction, because  $^{27}\text{Al}$  is a mirror nuclei of  $^{27}\text{Si}$ . The (d,p) reaction has a cross section of the order mb. Reaction theory allows to relate the (d,p) with the (p, $\gamma$ ) cross section.

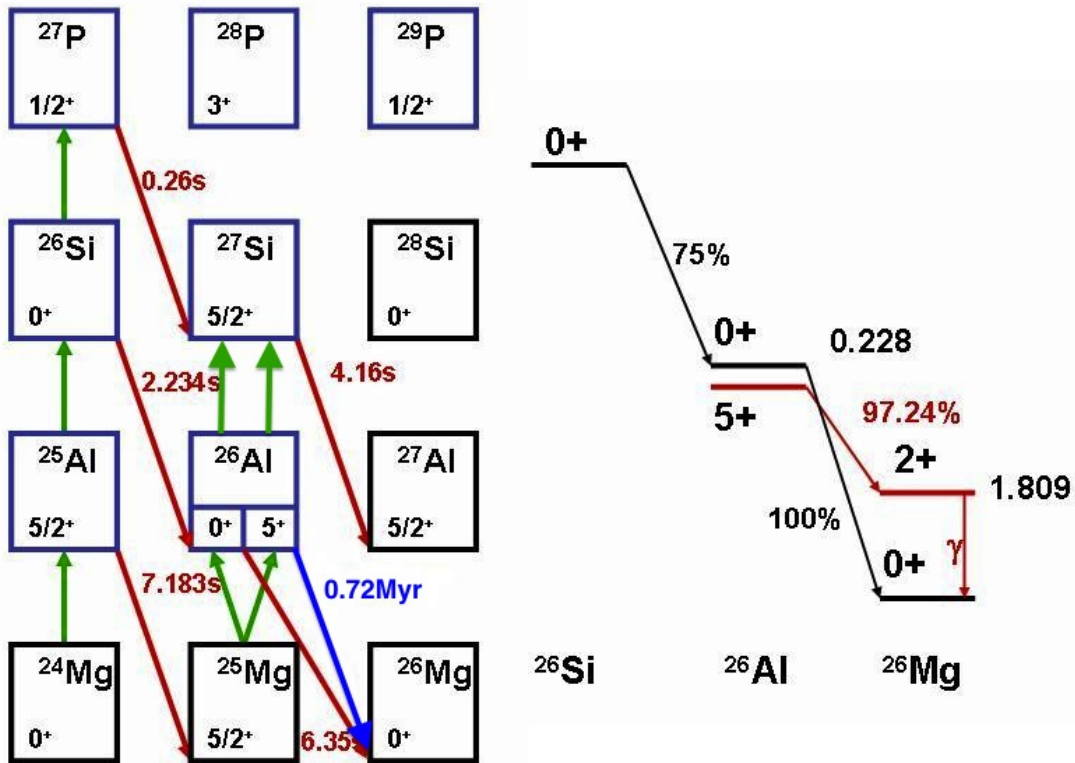
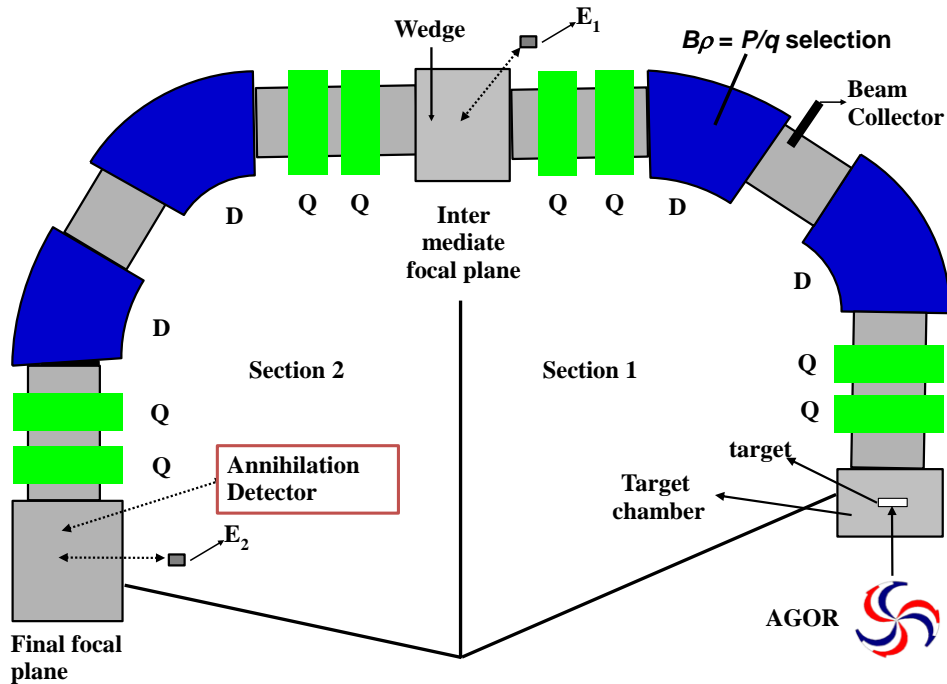


Figure 2: Decay scheme of  $^{26}\text{Al}$ [6] (green lines are proton capture, red are  $\beta^+$  decay and blue is the long lived  $\beta^+$  decay)

Figure 3: Schematic of the Tri $\mu$ p Magnetic Separator

## 2 Expected Production of $^{26}\text{Al}$

A  $^{26}\text{Mg}$  beam of 24.7 MeV/u is at the entrance of the Magnetic Separator (see fig. 3) from the AGOR cyclotron and shot onto a  $\text{H}_2$  target. This then produces a  $^{26}\text{Al}[13+]$  beam of  $\sim 10$  MeV/u with secondary products, at the exit. To filter out some of the secondary products, a wedge is placed in the IFP (Intermediate Focal Plane). Simulations with the program Lise++ [2] are made to establish the settings for the separator.

The remaining isotopes are then transported from the IFP to the FFP (Final Focal Plane), with  $^{26}\text{Al}[13+]$  having an energy of  $\sim 10$  MeV. The produced  $^{26}\text{Al}[13+]$  beam has a calculated rate of  $1.45\text{e}+4$  [isotopes/s] at 1 pA.

A schematic of the Magnetic Separator can be seen in Figure 3. The blue blocks are the dipoles (D), the green blocks the quadrupoles (Q). AGOR is the cyclotron that supplies the  $^{26}\text{Mg}$  beam to the separator. Dipoles change the trajectory of isotopes according to their momentum and charge; quadrupoles focus the trajectories.

Without a wedge in the beam path, the separator is symmetric in an axis through the IFP. The beam is focused in the target chamber and the FFP, but in the IFP the beam is dispersed. By then varying the magnetic rigidity of the separator, one can select between isotopes with different P/q ratio.

When a wedge is put into the beam path in the IFP, the dispersed beam can be filtered. The wedge introduces a second order component, in addition to the first order stopping component

Target	$\text{H}_2$
Pressure	1400 Torr
Temperature	77K
Thickness	$5.8312 \text{ mg/cm}^2$

Table 1: Target properties

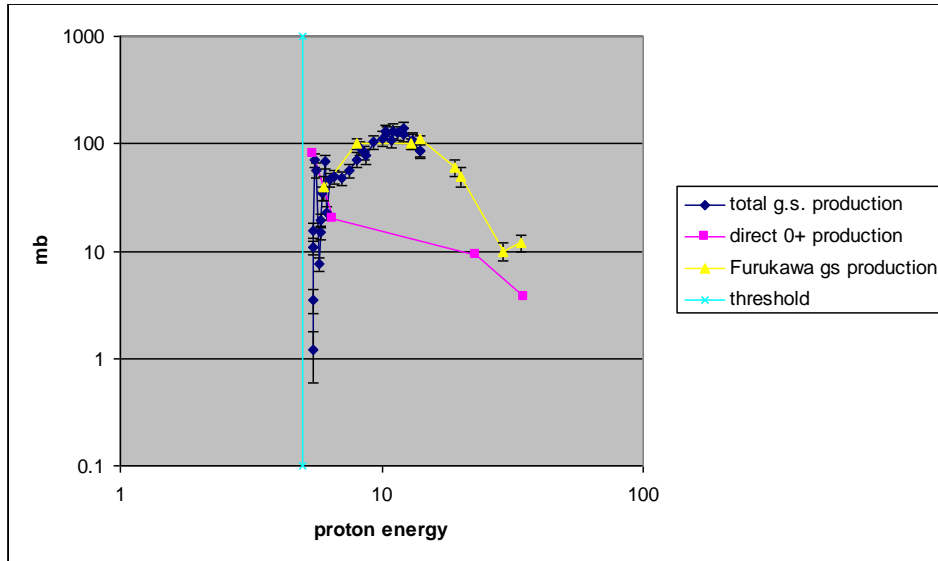


Figure 4: Cross-sections of the  $^{26}\text{Al}$  production reaction[1][3][10][5][11]

( $dE/dx$ ). Because stopping in a material is  $\propto \frac{Z^2}{v^2}$ , a selection in isotopes can again be made.

All calculated values are from the simulations with Lise++, a software package to create and simulate magnetic separators.[2] The separator at the KVI was imported to Lise++ and adjusted for an  $^{26}\text{Mg}$  beam. The target was set up using the settings in table 1.

In Lise++ the required reaction product can be selected, along with a reaction mechanism. Lise++ then calculates the required magnetic setting ( $B\rho$  values) and the estimated yield of the reaction. It also calculates the yields of secondary isotopes. To filter these secondary isotopes a wedge can be added to the setup. Lise++ can then estimate the required thickness of the wedge, if a wedge shape is known. The Tri $\mu$ p magnetic separator has three wedges in its setup, but the shapes of these wedges were not precisely known. Several points along the curved edge were taken to run a polynomial interpolation for the shape, and this shape was input into Lise++. The energies at the different stages of the separator and the Time-of-Flight (ToF) can also be calculated by Lise++.

A cross-section for the reaction was also needed. The  $^{26}\text{Mg}$  beam has an energy of 24.7 MeV/u, from Figure 4 it can be seen that the cross-section is  $\sim 10\text{mb}$ . This is the cross-section of  $^{26}\text{Al}^m$  (purple), and the cross section of  $^{26}\text{Al}^g$  (yellow/blue) is approximately 10 times as high.

There is a clear difference between the cross sections of the  $0^+$  state and the  $5^+$  state. The reaction at energies around 10MeV is a compound nucleus reaction, which has a cross section  $\sigma \propto \pi\lambda^2(2l+1)T$ , where T is the transmission coefficient. Since the ground state has a higher angular quantum number than the isomeric state, the cross section is higher. At higher energies a direct reaction component begins to contribute, while the compound nucleus reaction contribution falls off.

To use the output of the separator as a beam means that the experiment will have a mixture of  $^{26}\text{Al}^g$  and  $^{26}\text{Al}^m$  so that one has to run the experiment at two different energies to obtain different admixtures of  $^{26}\text{Al}^g$  and  $^{26}\text{Al}^m$ .

The beam energy of about 25 MeV was chosen to have a relative high  $^{26}\text{Al}^m$  yield that is fully stripped of electrons while the AGOR yield is high.

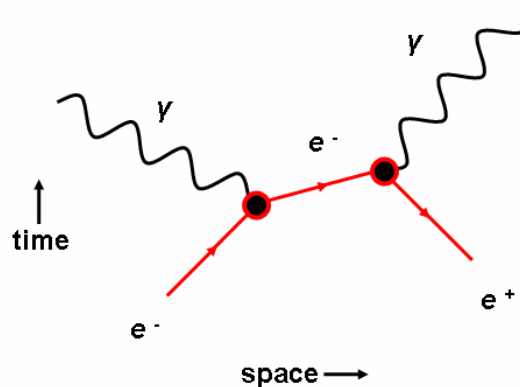
Detector settings	Det 1	Det 2
Course gain	500	50
Gain	1	1
Shaping time	.5 $\mu$ s	.5 $\mu$ s
Voltage	157V	80V
eV/channel	1.105e+04	1.353e+04

Table 2: Detector Settings

### 3 Detectors

#### 3.1 Annihilation Detectors

The annihilation detector is needed to observe the short lived  $^{26}\text{Al}^m$ . When it decays via  $\beta^+$ , the  $\beta$  isotope stops in material, interacts with an  $e^-$  and annihilates. This results in 2  $\gamma$  of 511 keV with  $180^\circ$  separation (Fig. 5) The annihilation detector consists of two  $\gamma$ -detectors placed on opposite sides of the FFP. (note that this is the principle of positron emission tomography).

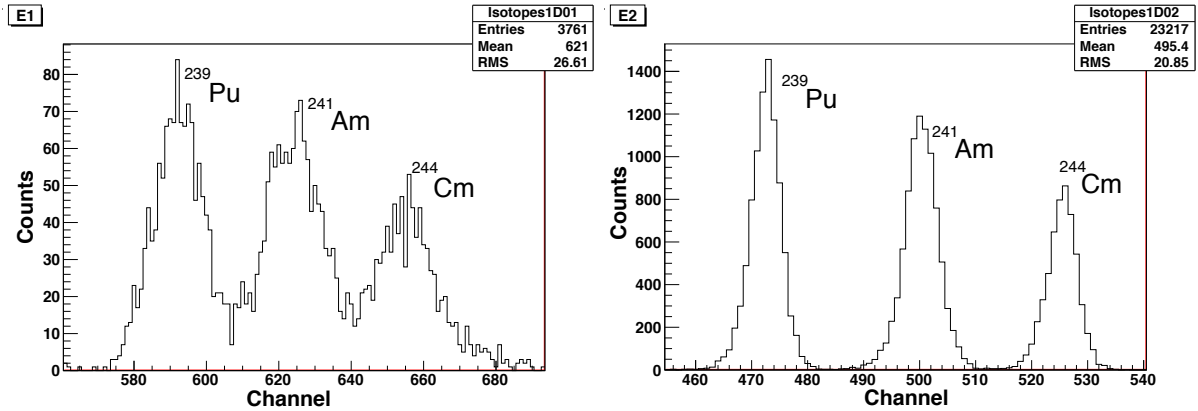
Figure 5: Feynman Diagram of annihilation of an  $e^-$  and an  $e^+$ 

##### 3.1.1 Calibration

Calibration of this detector is done by putting a  $^{22}\text{Na}$  source in the Faraday cup in the FFP.  $^{22}\text{Na}$  also decays via  $\beta^+$  emission. The  $\beta^+$  particles are stopped in the Faraday cup, and annihilate with  $e^-$ . Since the resulting  $\gamma$ 's are radiated isotropically, only a portion of the  $\gamma$ 's are detected, because the detector only picks up  $\gamma$ 's within a certain solid angle. With the given activity at the creation date and the life-time of the Na isotope, the current activity can be calculated. By comparing the current activity with the measured activity, the efficiency of the annihilation detection was found to be  $\sim 2.62 \times 10^{-3}$ . However, calibration with a source does not reproduce the actual experimental situation, the efficiency therefore should be determined more rigorously in any future experiment.

#### 3.2 Energy Detectors

Two semiconductors (Silicium) of  $300 \mu$  are used to measure the energy. The electrons are brought from the valence band into the conductance band by absorption of radiation. By creating an electric field in the semiconductors the electrons are then brought to the anode. One of the detectors is in the IFP (E1) and the other is in the FFP (E2).

Figure 6: Three  $\alpha$  peaks of Det 1 and Det 2;  $^{239}\text{Pu}$ ,  $^{241}\text{Am}$  and  $^{244}\text{Cm}$ 

Isotope	Energy
$^{239}\text{Pu}$	5.24MeV
$^{241}\text{Am}$	5.64MeV
$^{244}\text{Cm}$	5.90MeV

Table 3:  $\alpha$  decay energy of  $^{241}\text{Am}$  and contaminates

The silicon detectors are also used to measure the Time-of-Flight (ToF) between the target and the detector, using the radiofrequency signal of the cyclotron AGOR as a start.

### 3.2.1 Calibration

The energy detectors were calibrated by putting an  $\alpha$  source. (Table 3 and Figure 6) This is done by looking at the difference between mean of the gaussian decay peak and the offset when there is no signal. Since there is no signal, the offset is zero on the energy scale. The difference is then the energy of the  $\alpha$  isotope, and with this the energy per channel is calculated. The parameters of the detectors and amplifiers are in Table 2 for future reference.

### 3.3 ToF Detection

The dual AND configuration (Figure 7) is needed to ensure the full dynamic range of 20ns. (ToF can only be measured modulus  $1/\text{RF}$ , where RF is the radio frequency of AGOR) When there is only one AND the dynamic range is about 10ns due to the width of  $t_{\text{RF}}$ . This means there is a dead time of 10ns in which nothing can be measured. The dynamic range is most easily seen when there is no beam: then the ToF signal is a random signal. The time spectrum will be flat and 20ns long. If there is a beam, every 20ns a reaction can take place, and this is the start of the ToF measurement. Since the time measurement is modulus 20, a isotope that travels longer than 20ns will not show its actual ToF.



Figure 7: ToF circuit

## 4 Experiment

For the  $^{26}\text{Al}$  production, the target chamber was filled with  $\text{H}_2$  and cooled with liquid Nitrogen. The magnet current is setup by comparing the settings for a previous experiment,  $^{20}\text{Ne}$ , to the  $^{26}\text{Mg}$  Lise++  $B\rho$  values. Using the fact that  $B\rho$  is linearly proportional to the current, all settings were obtained by linear scaling.

The magnetic rigidity, or  $B\rho$ , of the magnets is a measure of how much the trajectories of the isotopes in the beam are curved.  $B\rho$  corresponds to a selection in  $P/q$ . So by scanning through the magnetic rigidity one can select the different isotopes in the beam, according to momentum  $P$  and charge state  $q$ .

From this point several measurements are done at different  $B\rho$  values to optimize the  $^{26}\text{Al}$  yield by looking at the rate of detection in the energy detector in the IFP. When it is optimized in the IFP, the next step is optimization in the FFP. In the FFP one looks at both the energy detector as well as the annihilation detector.

Because there are also other isotopes in the  $^{26}\text{Al}$  beam, using the annihilation detector it can be seen which one is the unstable  $^{26}\text{Al}$  and which ones are the other stable isotopes in the energy spectrum, and optimize the settings using the annihilation detection rate.

After this the  $160\mu\text{Al}$  wedge is put in, and again using the values of  $B\rho$  given by Lise++, the magnet settings in section 2 are scaled. The settings for section 1 remain the same, since the energy of the isotopes now changes in the IFP, which is after section 1.

By again scanning through  $B\rho$  values for section 2, and looking at the annihilation rate and energy spectrum the settings are optimized.

## 5 Data Analysis

By looking at a graph of energy versus Time of Flight (ToF) several 'islands' can be seen. (Figure 16) Each island represents a isotope with a certain energy and ToF. However, certain isotopes can overlap each other because they have the same energy and slightly different ToF. This happens with  $^{26}\text{Al}$ , which has a ground state and a isomeric state.

Since the ground state has a half-life of 0.717Myr, and the isomeric state a half-life of 6.3s, the component of the ground state for the annihilation measurement is negligible compared to  $^{26}\text{Al}^m$ .

### 5.1 Intermediate Focal Plane

Because  $^{26}\text{Al}$  needs to be identified, the next measurements were done in the FFP where, in addition the the energy detector, the annihilation detectors are situated. Which island is  $^{26}\text{Al}$

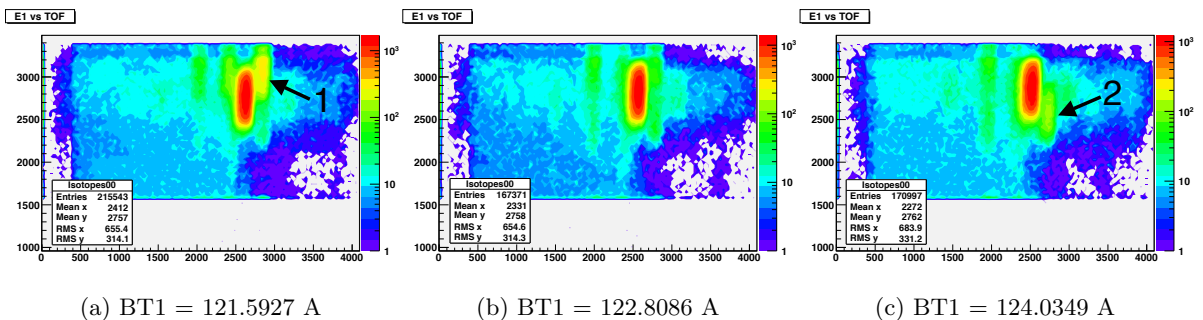


Figure 8: 2D histograms of E1 vs ToF vs counts

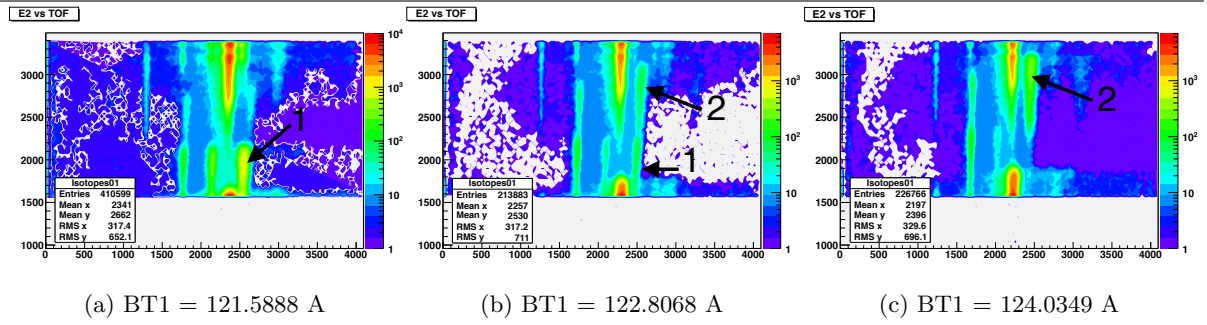


Figure 9: 2D histograms of E2 vs ToF vs counts

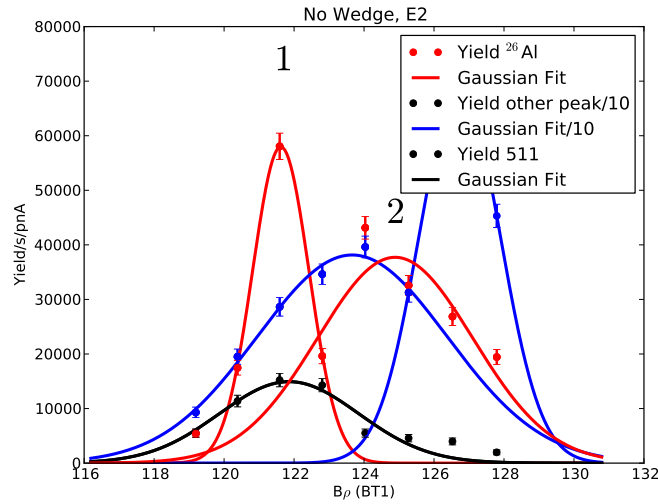


Figure 10: Yield with no wedge in E2

can be identified using the annihilation yield, since according to simulations all contaminants are stable.

## 5.2 Final Focal Plane

By integrating the counts in a peak in Figure 11b, which is a projection of Figure 11a onto the x-axis, one acquires the total number of events during the measurement. This is then normalized to beam current and per time unit to get the yield/s/pnA. The events in the annihilation detector are also normalized to beam current and per time unit, and this is plotted against the rigidity of the magnets ( $B\rho$ ) to see for which setting the yield is maximal. (Figure 12a)

The same procedure was also used for the data from the measurement without a wedge, and plotted to find the rigidity setting for the maximal yield. There are two peaks in the projection of in Figure 9 onto the x-axis, and again there are two different isotopes in those two peaks. (Figure 9, peaks 1 and 2). Two of the isotopes are clearly not  $^{26}\text{Al}$ , since their maxima are too high (Fig. 4), and also do not coincide with the annihilation maximum. (Blue lines and points in Figure 10) The yield is too high since from Figure 4 it can be seen that the ratio between the  $0^+$  and  $5^+$  state is 10/30, so 25% is in the  $0^+$  state.

The other two isotopes that remain (peaks number 1 and 2 in Figure 10) have yield maxima that could be connected to the annihilation maximum, but peak 2 clearly has its maximum at a different magnetic rigidity setting. When looking at Figure 9 an astute observer would notice that the position of the two isotopes has switched. Isotope number 1 ( $^{26}\text{Al}$ ) now has a lower

ToF than isotope 2, while the reverse was true in E1. This is a side-effect of the wraparound of the ToF detector. Because the isotopes in E2 have a longer travel time, in the case of  $^{26}\text{Al}$  longer than the wraparound time, it shows up at lower ToF, but it actually has a higher ToF than isotope 2.

The yield of  $^{26}\text{Al}$  in E2 is  $\sim 5.8 \times 10^4$  /s/pnA.

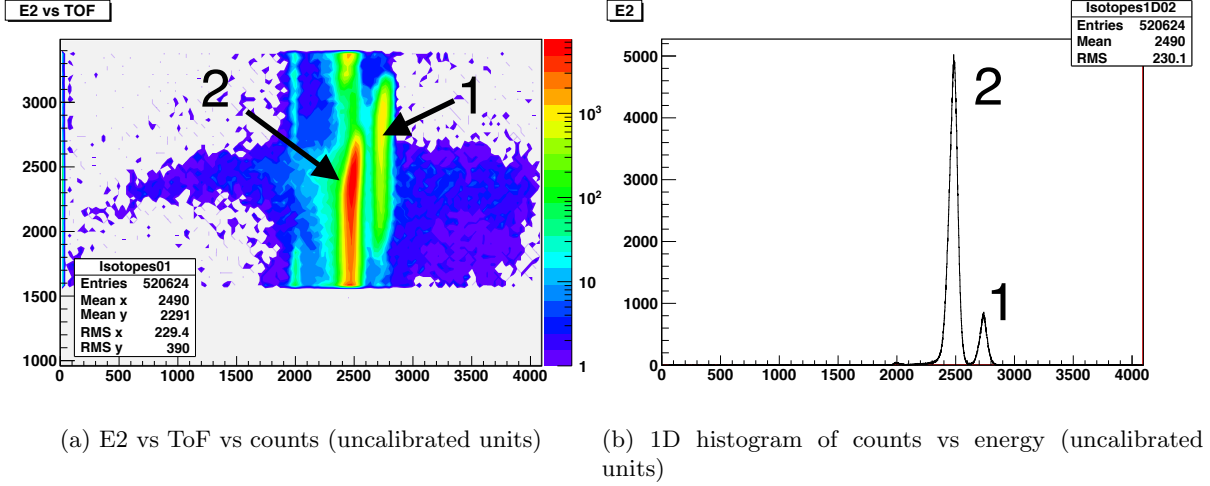


Figure 11: Graphs with data of the  $160\mu$  wedge run

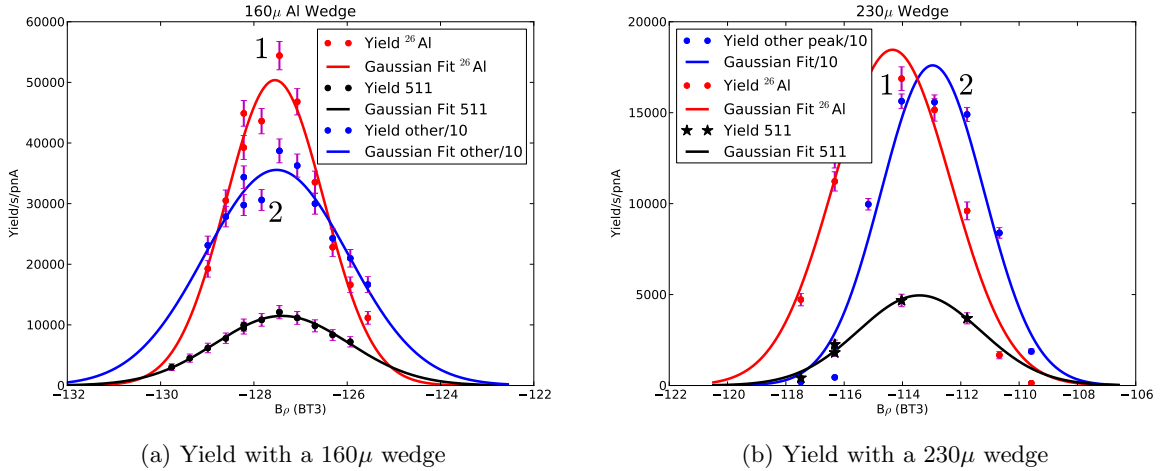


Figure 12: Yield with wedges

Figures 11 and 12a are for the  $160\mu$  wedge run. To identify which isotope is  $^{26}\text{Al}$  the positions of the yield maxima cannot be used, since they are approximately the same. But because it is known that with this reaction  $\sim 25\%$  of the total  $^{26}\text{Al}$  is in the  $0^+$  (isomeric) state, peak number 1 in Figure 11b is the  $^{26}\text{Al}$  peak. Peak number 2 has a yield that is too high to correspond to the annihilation rate. With a  $160\mu$  wedge the total  $^{26}\text{Al}$  yield is of  $\sim 5 \times 10^4$ /s per pnA. This would give a yield of  $\sim 1.25 \times 10^4$ /s per pnA for  $^{26}\text{Al}^m$ . This is  $\sim 86\%$  of the yield without a wedge, but the resulting beam is cleaner.

From Figure 12a it can clearly be seen that this is not the measured annihilation yield. The  $\beta^+$  have too much energy to fully stop in the faraday cup, and as a result some go through the

material of the faraday cup, and consequently do not annihilate within the field of view of the detectors.

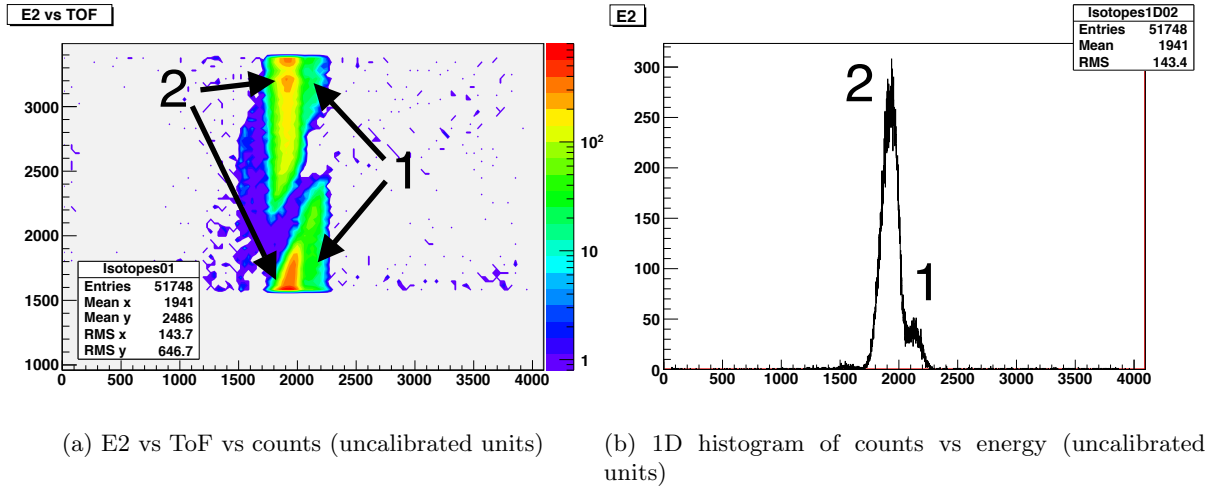


Figure 13: Graphs with data of the  $230\mu$  wedge run

The measurement was also done for a  $230\mu$  wedge, as can be seen in Figure 13. There are again two peaks in the energy spectrum, but some of the background is filtered out and the  $^{26}\text{Al}$  peak is somewhat lower. The  $^{26}\text{Al}$  peak and peak number 2 also overlap each other now. The width of the two peaks is also larger.

By integrating, normalizing and scaling the data from Figure 13, the yield/s/pnA can again be plotted (Fig. 12b). The yield with a  $230\mu$  wedge is  $\sim 1.8 \times 10^4$  isotopes/s/pnA  $^{26}\text{Al}$ , and this gives a  $^{26}\text{Al}^m$  yield of  $\sim .45 \times 10^4$  isotopes/s/pnA.

This is  $\sim 31\%$  of the yield without a wedge, and the resulting beam has overlapping isotopes. The energy resolution is also decreased, due too the stopping of the wedge which causes a wider range of isotope energies. So it can be seen that the  $160\mu$  wedge gives a better beam.

It is clear that peak number 2 has the same P/q value as  $^{26}\text{Al}$ , since it cannot be separated by varying the magnetic rigidity. From the fact that  $^{26}\text{Al}$  loses more energy with a thicker wedge than peak number 2, and using Bethe-Bloch (stopping  $= \propto Z^2/v^2$ ), one can infer that peak number 2 has to be  $^{24}\text{Mg}$ . The life-time measurement (Figure 14) gave a  $\tau_{1/2}$  of  $6.22 \pm 0.50$ s, consistent with the  $^{26}\text{Al}^m$  lifetime.

### 5.3 Back to the Intermediate Focal Plane

With the annihilation yield from the FFP, the IFP data is analyzed. Again the count rates for different magnetic rigidities are integrated over the different peaks and normalized. Then the yield is plotted versus the magnetic rigidity, including the annihilation yield.

In E1 there are multiple peaks that need to be identified. By comparing the peaks to the annihilation peak, the  $^{26}\text{Al}$  peak can be identified. In Figure 15a the three rightmost peaks in Figure 15b are integrated for all  $B\rho$  measurements. However the second and third peak from the right cannot be  $^{26}\text{Al}$  since for the third peak from the right, the maximum yield does not coincide with the maximum of the annihilation measurement and the second peak from the right has a yield that is too high to be connected to the annihilation measurement. The yield is too high since it is known that with this reaction  $\sim 25\%$  of the total  $^{26}\text{Al}$  is in the  $0^+$  (isomeric) state (Fig. 4), and this is clearly not true for this peak.

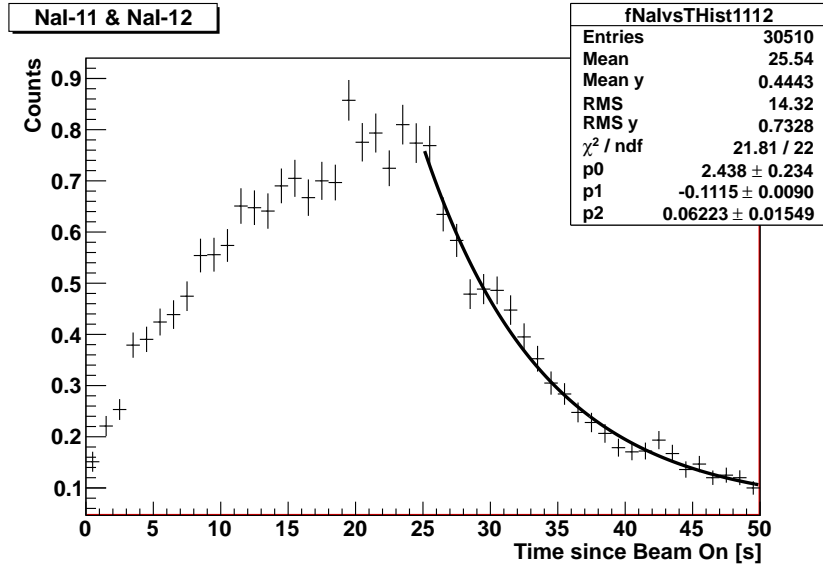
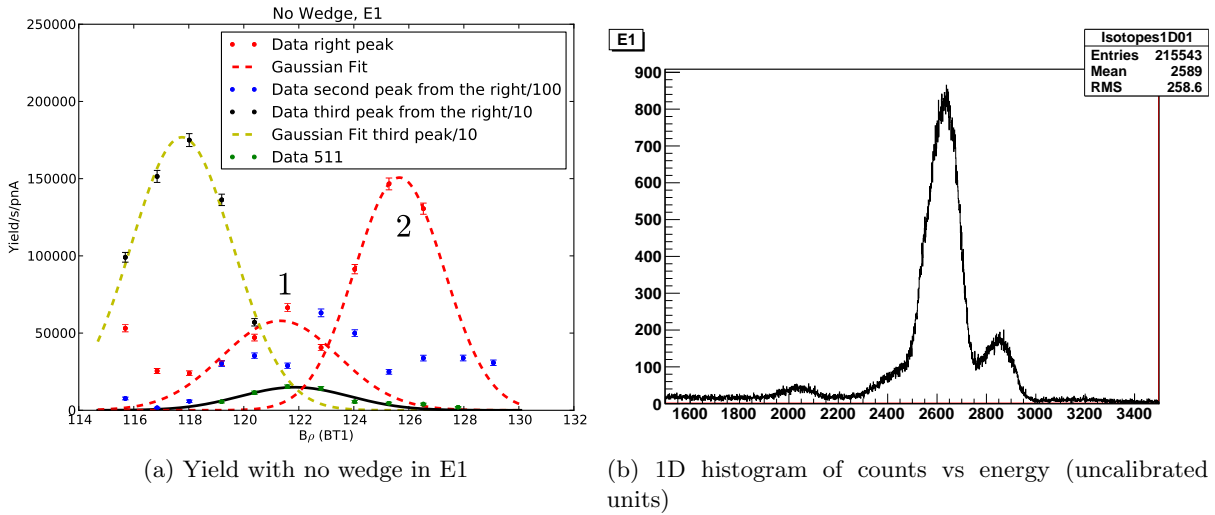
Figure 14: Exponential plus background fit for the lifetime,  $\tau_{1/2} = 6.22 \pm 0.50\text{s}$ 

Figure 15: 1D graphs of E1

The only option left is the rightmost peak, but it has several maxima at different  $B\rho$ , as seen in Figure 15a (peak number 1 and 2). These two maxima can also be seen in Figure 16, where Figure 16a corresponds to peak number 1 and Figure 16c corresponds to peak number 2 in Figure 15a.

The right peak yield (red in Fig. 15a) has been scaled upward by a factor to compensate for the closed slits. The closed slits influence the momentum acceptance, causing it to be lower resulting in a lower count rate. So in order to get the true yield it was scaled upward by a factor that is the average between ratios of annihilation yields with the  $^{26}\text{Al}$  yields at  $160\mu$  and  $230\mu$ .

Concluding, this means that only the part of the yield curve with the maximum coinciding with the annihilation maximum is  $^{26}\text{Al}$ . At BT1 higher than 123 A and lower than 118 A a different isotope enters the detector, and is dominating the  $^{26}\text{Al}$  contribution.

This gives a  $^{26}\text{Al}$  yield of  $\sim 5.8 \times 10^4$  isotopes/s/pnA in E1. This number is not very certain, since it has been scaled by a factor that is itself not very precise. Taking into account that  $\sim 25\%$

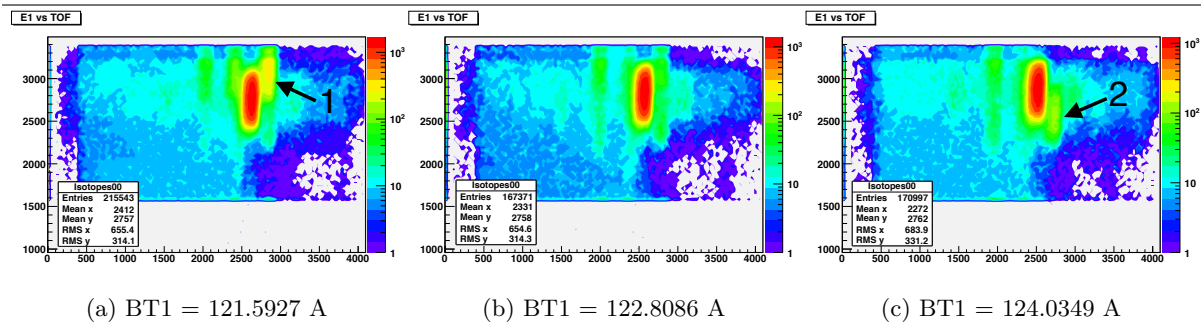


Figure 16: 2D histograms of E1 vs ToF vs counts

of the total  $^{26}\text{Al}$  is in the  $0^+$  state(Fig. 4), this gives a  $^{26}\text{Al}^m$  yield of  $1.45 \times 10^4$  isotopes/s/pnA.

## 6 Conclusion

The production of isomeric  $^{26}\text{Al}$  was studied, to see if it can be used as a radioactive beam for astrophysical studies. With the method described here a secondary beam was produced with sufficient intensity to make such a study possible.

This study shows that for a typical beam of 100 nA  $^{26}\text{Mg}$ ,  $1.25 \times 10^6$ /second  $^{26}\text{Al}^m$  isotopes can be produced with a contaminant,  $^{24}\text{Mg}$ , that has a significantly higher yield than  $^{26}\text{Al}$ . This significantly complicates experiments aimed at measuring  $^{26}\text{Al}^m$  induced reactions.

## 7 Acknowledgements

I would like to thank my advisor, Prof. Dr. Hans Wilschut, for his help during the preparation and execution of the experiment.

I would also like to thank the operators of the AGOR cyclotron for providing a reliable beam.

---

**References**

- [1] J. D. Carlson, C. D. Zafiratos, and D. A. Lind. Optical model analysis of quasielastic (p, n) reactions at 22.8 mev. *Nuclear Physics A*, 249(1):29 – 62, 1975.
- [2] D.Bazin, O.B.Tarasov, M.Lewitowicz, and O.Sorlin. Lise++. <http://groups.nsc1.msu.edu/lise/lise.html>, May 2011.
- [3] G. Doukellis and J. Rapaport. The 26mg(p, n)26al and 23na([alpha], n)26al reactions near threshold. *Nuclear Physics A*, 467(3):511 – 527, 1987.
- [4] Max-Planck-Institute for Astrophysics. Sky map of the 1809mev line of <sup>26</sup>Al. <http://www.mpe.mpg.de/xray/research/gallery/calendar/Kal2003/dec.php?lang=en>, December 2003.
- [5] M. Furukawa, K. Shizuri, K. Komura, K. Sakamoto, and S. Tanaka. Production of 26al and 22na from proton bombardment of si, al and mg. *Nuclear Physics A*, 174(3):539 – 544, 1971.
- [6] USC GENP. <sup>26</sup>Al scheme. <http://fpsalmon.usc.es/genp/doc/nuclear/experiments/s223/astrophysics.shtml>, Juli 2011.
- [7] H.Wilschut G.Lotay. Kvi proposal p19, Juli 2011.
- [8] J. Knödseder. On the origin of galactic <sup>26</sup>Al. *Astrophysical Letters Communications*, 38:379–+, February 1999.
- [9] Brookhaven National Laboratory. United states national nuclear data center. <http://www.nndc.bnl.gov/>, May 2011.
- [10] Eric B. Norman, Kevin T. Lesko, Timothy E. Chupp, and Peter Schwalbach. 26gal production cross sections from the 26mg(p, n)26al reaction. *Nuclear Physics A*, 357(1):228 – 236, 1981.
- [11] H. Orihara, A. Terakawa, K. Itoh, H. Suzuki, K. Kumagai, Y. Kikuchi, G. C. Jon, K. Ishii, T. Niizeki, H. Sagawa, and H. Ohnuma. Gamow-teller matrix elements in light nuclei and (p,n) cross sections at  $E_p = 35$  MeV. *Physics Letters B*, 539(1-2):40 – 45, 2002.
- [12] James R. Simanton, Robert A. Rightmire, Alton L. Long, and Truman P. Kohman. Long-lived radioactive aluminum 26. *Phys. Rev.*, 96(6):1711–1712, Dec 1954.

## List of Figures

1	Sky map of the 1809MeV $\gamma$ line of $^{26}\text{Al}$ [4] . . . . .	1
2	Decay scheme of $^{26}\text{Al}$ [6] (green lines are proton capture, red are $\beta+$ decay and blue is the long lived $\beta+$ decay) . . . . .	3
3	Schematic of the Tri $\mu$ p Magnetic Separator . . . . .	4
4	Cross-sections of the $^{26}\text{Al}$ production reaction[1][3][10][5][11] . . . . .	5
5	Feynman Diagram of annihilation of an $e^-$ and an $e^+$ . . . . .	6
6	Three $\alpha$ peaks of Det 1 and Det 2; $^{239}\text{Pu}$ , $^{241}\text{Am}$ and $^{244}\text{Cm}$ . . . . .	7
7	ToF circuit . . . . .	7
8	2D histograms of E1 vs ToF vs counts . . . . .	8
9	2D histograms of E2 vs ToF vs counts . . . . .	9
10	Yield with no wedge in E2 . . . . .	9
11	Graphs with data of the 160 $\mu$ wedge run . . . . .	10
12	Yield with wedges . . . . .	10
13	Graphs with data of the 230 $\mu$ wedge run . . . . .	11
14	Exponential plus background fit for the lifetime, $\tau_{1/2} = 6.22 \pm 0.50\text{s}$ . . . . .	12
15	1D graphs of E1 . . . . .	12
16	2D histograms of E1 vs ToF vs counts . . . . .	13

## List of Tables

1	Target properties . . . . .	4
2	Detector Settings . . . . .	6
3	$\alpha$ decay energy of $^{241}\text{Am}$ and contaminates . . . . .	7